

Seasonal cycles of surface layer salinity in the Pacific Ocean

F. M. Bingham¹, G. R. Foltz², and M. J. McPhaden³

¹Center for Marine Science, Univ. of North Carolina Wilmington, 601 S. College Rd., Wilmington, NC 28403-5928, USA

²Joint Institute for the Study of Atmosphere and Ocean, Univ. of Washington, 3737 Brooklyn Ave NE, P.O. Box 355672, Seattle, WA 98105-5672, USA

³NOAA/Pacific Marine Environmental Laboratory, 7600 Sand Point Way NE, Seattle, WA 98115, USA

Received: 24 August 2009 – Published in Ocean Sci. Discuss.: 26 October 2009

Revised: 28 July 2010 – Accepted: 9 August 2010 – Published: 24 August 2010

Abstract. The seasonal variability of surface layer salinity (SLS) is examined in the Pacific Ocean between 40° S and 60° N using a variety of data sources. Significant seasonal cycles were found in 5 regions: 1) The western North Pacific, 2) The northeastern North Pacific and Alaska gyre, 3) the intertropical convergence zone (ITCZ), 4) an area of the central North Pacific north of the Hawaiian Islands, 5) the central South Pacific along 10–20° S. Amplitudes range from 0.1 to > 0.5. The largest amplitudes are in the tropical band and the western North Pacific. Maximum salinity is obtained in late (northern) winter in the western North Pacific, late winter and early spring in the northeastern North Pacific, early summer in the ITCZ area, late summer and early fall in the central North Pacific area and (austral) winter in the central South Pacific. Large areas of the Pacific have no significant seasonal variation in SLS.

Seasonal variability of evaporation rate, precipitation rate and the difference between them (E-P) were calculated from the OAFflux and Global Precipitation Climatology Project datasets. Typical amplitudes of E-P are $0.1-1 \times 10^{-4} \text{ kg m}^{-2} \text{ s}^{-1}$. The seasonal variability of E-P is largely dominated by variability in evaporation in the western North Pacific and precipitation elsewhere. The largest amplitudes are in areas along the edge of the western North Pacific and in the far eastern tropical Pacific around 10° N. Phases in these areas indicate maximum E-P in mid- to late winter in these areas of large amplitude. The closest correspondence between E-P and SLS is in the ITCZ. E-P was combined with seasonal variation of the mixed-layer depth to calculate the freshwater flux forcing term of the SLS balance equation. The term was found to be similar in magnitude

and distribution to E-P. Some other terms of the SLS balance were calculated. Horizontal advection was found to have seasonal cycles in a region near the equator. Entrainment was found to be mostly not significant except for a small region along 2.5–7.5° N in the eastern Pacific.

Averaged spatially over large areas in the western North Pacific, ITCZ, South Pacific and northern North Pacific, the seasonal cycle is mostly a balance between changes in SLS and E-P, with entrainment and advection playing relatively minor roles.

This work highlights the potentially significant role of surface salinity in the hydrologic cycle and in subtropical mode water formation. It can also help to interpret measurements that will soon be available from the Aquarius and SMOS (Soil Moisture and Ocean Salinity) satellite missions.

1 Introduction

It has long been understood that the ocean outside the tropics undergoes a seasonal cycle in surface temperature, getting warmer in summer/fall and cooler in winter/spring. The reasons for this are obvious, with a strong seasonal signal in solar radiation. Seasonal changes in surface layer salinity (SLS) over the open ocean are much less well understood. SLS in the ocean is affected by evaporation, precipitation, entrainment, advection and mixing (Delcroix et al., 1996). Any one of these components might be expected to have seasonal variability, especially precipitation or evaporation. We would most expect to see seasonal signals in SLS in areas that have seasonal signals in evaporation and precipitation, such as areas of mode water formation and near zones of seasonally varying rainfall like the intertropical convergence zone (ITCZ).



Correspondence to: F. M. Bingham
(binghamf@uncw.edu)

The mode water formation process has been described in a number of places (e.g. Hanawa and Talley, 2001). It is thought to be largely a result of evaporative cooling and thickening of the surface mixed layer in wintertime. Evaporation leads not only to cooling, but also to salinification, which in turn leads to increased density. To understand mode water formation it is therefore important to assess the roles of both temperature and salinity. Quantifying the seasonal cycle of salinity in mode water formation regions can help to clarify the role played by salinity and evaporation in the mode water formation process.

In the near future, two satellite missions, Aquarius (Lagerloef et al., 2008) and SMOS (Soil Moisture and Ocean Salinity; Berger et al., 2002) will begin to measure surface salinity from space. (As of this writing, SMOS has successfully launched and is beginning to return data.) To better understand satellite retrievals, it will be necessary to know the seasonal cycle of surface salinity as these will be among the earliest signals to emerge from the satellite datasets. Areas with strong seasonal variability are good candidates for intensive calibration and validation activities for the missions.

The seasonal variability of SLS has been most intensively studied in the tropical Pacific (e.g. Delcroix et al., 1996; Delcroix and Henin, 1991, henceforth DH91; Delcroix et al., 2005). DH91 looked at seasonal variability averaged from bucket data along a series of volunteer observing ship tracks in the tropical Pacific. They found maximum variability in the ITCZ in the Northern Hemisphere and along 8–10° S in the Southern Hemisphere, with SSS minima in September–October and March–April, respectively. The method they used to determine the seasonal cycles was to find the standard deviation for each month away from the mean yearly values for a particular latitude. The maximum standard deviations they found were 0.13–0.38 increasing in size and latitude from west to east. They calculated the seasonal cycles of precipitation for each of the lines to understand the relationship between rainfall and SSS. They found, as expected, that the maximum in precipitation in the South Pacific and ITCZ led the minimum in SLS by three months, leading them to conclude that the seasonal cycle in those areas was largely driven by precipitation. There was a strong maximum in the seasonal cycle along their eastern track north of the equator, near 90° W. They attributed this maximum to a combination of precipitation, evaporation and horizontal and vertical advection of salt. In examining the role of advection of salt in the seasonal SSS budget, they concluded that there was not sufficient information to make any judgment on the importance of geostrophic advection, but that seasonal Ekman advection was in phase with rainfall. DH91 examined seasonal cycles of SLS along some specific lines in limited areas, but did not include any estimate of the uncertainty of their calculations. Nevertheless, their results are largely consistent with what we will show in this paper over a much larger area.

Delcroix et al. (1996) also examined seasonal variations of SLS and compared them with precipitation measurements.

They decomposed the basin-wide SLS data into ENSO-scale first mode and seasonal second mode empirical orthogonal functions (EOFs). The seasonal mode accounted for 17% of the variance. The seasonal mode (their Fig. 6) included a maximum in variability at close to 10° N in the eastern tropical Pacific, trending toward the equator towards the west. A much stronger and oppositely-phased maximum was observed in the South Pacific at around 15° S, 170° W. At the same time, they found a similarly-structured first mode EOF in precipitation. The precipitation EOF led the (negative of the) SLS EOF in phase by about 2 months, with the precipitation reaching a minimum in July–August and the SSS a maximum in September–October. They concluded that precipitation was the most important process governing SLS in the tropical Pacific. However, a spatial offset in the peaks of SLS and precipitation variability in the South Pacific implied that precipitation was not the only process controlling SLS on the seasonal time scale (Gouriou and Delcroix, 2002; Johnson et al., 2002).

The results of Delcroix et al. (1996) are dependent upon the use of EOFs which unify the entire tropical Pacific basin. A simpler analysis is attempted here assuming no connection between SLS variations in the various areas of the North and South Pacific. We attempt to find the phase and amplitude wherever a significant signal may exist.

Delcroix et al. (2005) examined the seasonal cycle along a number of repeating volunteer observing ship tracks in the Pacific (and Atlantic and Indian) Ocean using mainly VOS data. They found that the seasonal cycle was most pronounced in the area under the ITCZ, accounting for over 50% of the variance in this latitude band. Their analysis focused on only the latitudes equatorward of 30° and only on the SLS itself, not on evaporation and precipitation. We will do a similar analysis here, only in a larger area of the tropical and mid-latitude Pacific from 40° S to 60° N. We will also evaluate the contribution of E-P.

In the Atlantic, Foltz and McPhaden (2008) calculated the salinity balance in three large areas, one in the central North Atlantic with weak seasonal variability and two in the tropical and western North Atlantic with larger seasonal variability. Their approach was to use large boxes and calculate mixed-layer salt budgets. They found that the contributions to the budgets were quite varied. In the central tropical Atlantic, the seasonal cycle of SLS was mainly influenced by seasonal variation in precipitation driven by migration of the intertropical convergence zone. In the western tropical Atlantic, salinity advection was the dominant process. In the central North Atlantic, a weak seasonal cycle in SLS was mainly a balance between advection and precipitation.

Johnson et al. (2002) calculated horizontal divergence of SSS in the global tropics in the mean and on a seasonal time scale using the 1994 World Ocean Atlas (Levitus et al., 1994) and the OSCAR surface currents (Bonjean and Lagerloef, 2002). They found the seasonal divergence to be a significant fraction (53%) of the annual mean divergence. The

calculation was done using a relatively large smoothing scale (9.8° longitude, 2.3° latitude) and did not include local salinity change or E-P on the seasonal scale. They did find seasonal variations in the divergence in the tropical oceans, especially underneath the ITCZ.

In the most comprehensive study of seasonal variability of SLS, Boyer and Levitus (2002) published maps of seasonal cycles on a global scale based on the 1998 World Ocean Atlas monthly gridded values (Boyer et al., 1998). The results they found are similar to what we will show in the Pacific. Our work is different from theirs in a couple of ways. Boyer and Levitus did not attempt to apply harmonic analysis to individual data, but to monthly gridded values. Thus, they may have lost some of the smaller scale detail in the amplitudes and phases. They did not show the statistical significance of the harmonic amplitudes. Just as important as the amplitude and phase of the seasonal cycle is to determine the places in the ocean where seasonal cycles do not exist or cannot be determined by current data. A significant number of new data have been collected since their work, mainly through profiling floats, that are incorporated here. Finally, they did show the seasonal cycles of E-P, but did not estimate horizontal advection, which we will attempt as well.

Until recently, the seasonal variability of SSS has been difficult to quantify over the open ocean. Salinity measurements have been limited to specific locations or ship tracks, and coverage over the entire range of seasons has been limited. Recently, however, the Argo program (Roemmich et al., 2009) has deployed profiling floats which measure profiles in quasi-random locations over a wide area. Now that Argo has been running for several years it has become possible to use these and other observations to examine variability on many time scales. As several realizations of the annual period have been measured, we can now determine the seasonal cycle of salinity and E-P, and explicitly determine the amplitude and phase and their statistical significance. Since the data are available, we take the approach of not averaging over a set of large areas (Foltz and McPhaden, 2008; Ren and Riser, 2009), using EOFs (Delcroix et al., 1996), gridded climatologies (Boyer and Levitus, 2002) or of focusing on specific ship tracks (DH91) but of looking at the seasonal cycle in detail over a large area. This allows us to get a closer picture of areas of interest like the mode water formation regions and the ITCZ. We also examine terms of the SLS budget to see what the balance is on a seasonal time scale.

In this paper we have focused on the Pacific basin between 40° S and 60° N. There are a couple of reasons for this. There is a large concentration of SLS data in the region, from volunteer observing ship lines, Japanese hydrographic surveys, Argo floats and other sources. There have been some previous studies of seasonal variability of SLS in the region, and we are building from those to provide a regional focus and to put the previous studies in a basinwide perspective.

2 Data and methods

The data used in this study depict several different phenomena, SLS, evaporation and precipitation. In addition, for our calculations we have used mixed-layer depth (MLD) and current data to determine seasonal cycles of some of the terms in the surface salt balance. We now describe the origin and methods used for each dataset.

2.1 Data sources

The following describes the sources for the SLS, mixed-layer depth, precipitation, evaporation and surface current data. Since each of the sources are averaged onto a slightly different grid, all datasets were subsampled or averaged onto a common $2.5^\circ \times 2.5^\circ$ grid. World Wide Web addresses for all data sources are provided in the acknowledgements.

2.1.1 Surface layer salinity

The SLS data used in this study come from several sources, the 2005 World Ocean Database (WOD05), EPIC CTD data, French LEGOS data, Argo and the TAO-TRITON moorings.

2.1.2 WOD05

The 2005 World Ocean Database (WOD05) (Johnson et al., 2006) contains several data files in the Pacific. In this paper we used the ocean station data (Fig. 1c; OSD) file. The WOD05 CTD file was not used as CTD data are included in a low-resolution version in the OSD file. For each profile in each of these files, we picked out the topmost value of salinity as the value of SLS, as long as that value was at 10 m depth or shallower and the observation was flagged as good in the file. The distribution of the OSD data in Fig. 1c indicates that they are heavily concentrated in coastal areas near the US in the eastern North Pacific, Japan in the western North Pacific, and a few other areas.

In addition to the WOD05, we used the World Ocean Atlas 2009 (Antonov et al., 2010) annual mean salinity field to calculate mean vertical salinity gradient for use in calculation of entrainment.

2.1.3 LEGOS

The LEGOS (Laboratoire d'Etudes Geophysiques et Oceanographiques Spatiales) validated data include surface bucket and underway thermosalinograph data from 30° S– 30° N, 1950–2003 in the Pacific (Fig. 1b). These observations are heavily grouped along major shipping lanes. See Delcroix et al. (2005) for discussion of data origin and validation procedures. The depths represented by these data range from the surface using a bucket to a few meters from a thermosalinograph. Adjustment was made in this study for variations in sample depth or collection method. Delcroix et al. (2005) subtracted 0.1 from all bucket salinities and added

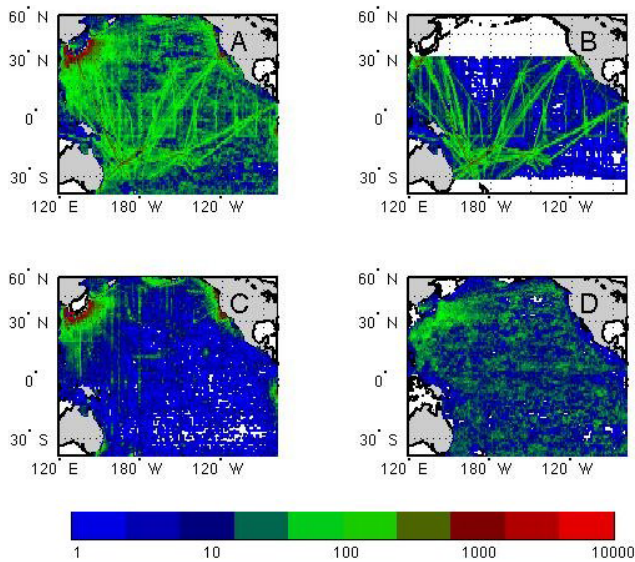


Fig. 1. Spatial distribution of SLS observation density, number of observations/one degree square. Color scale is shown at bottom. (a) All data. (b) Legos Data. (c) OSD data. (d) Argo data. Note color scale is logarithmic. Note also that there was considerable overlap between the original datasets, particularly Legos and OSD. This figure depicts the final data after removal of duplicate measurements.

0.02 to all thermosalinograph measurements to account for the different techniques. We followed this practice for data obtained from LEGOS but not from other data sources.

2.1.4 EPIC

EPIC is the data management system for oceanographic data taken during various NOAA cruises. From this system, we extracted CTD data from our Pacific domain at 5 m depth. The cruises where these data were taken were mostly servicing missions for the TAO array. The number of data from this source was small compared to other sources (Fig. 2).

2.1.5 Float data

Argo float profiles were gathered from the NODC (National Oceanographic Data Center) Argo data repository. Data from the repository from the period January 1996–December 2009 are used in this study with quality control flags of either 1 or 2. The Argo data added about 240 000 observations to the ensemble. Float data have the advantage over the other datasets in that the spatial distribution is quite uniform (Fig. 1d).

2.1.6 Combined data

Once the above four datasets were extracted, they were combined into one large ensemble, taking care to screen for duplicates. There was some duplication, especially between the LEGOS and OSD data. The final dataset is made up of ap-

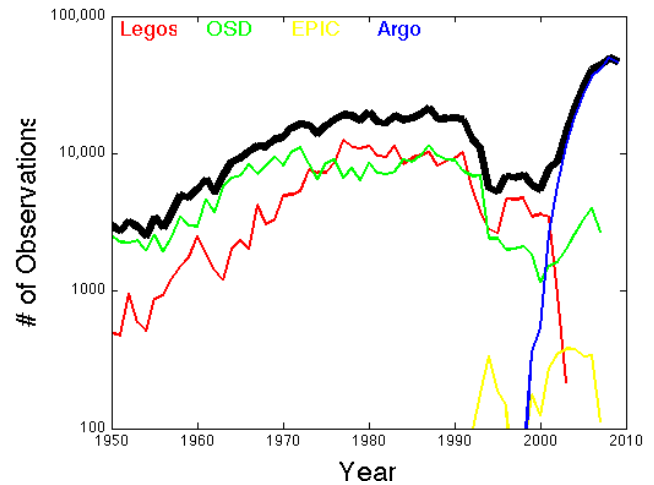


Fig. 2. Time distribution of SSS observations per year in the final dataset. Different colored lines are matched with text at the top of the figure to show which dataset is being plotted. The thick black line is the total for all observations. Note the ordinate is logarithmic. Note also that there was considerable overlap between datasets, particularly Legos and OSD. This figure depicts the final dataset after removal of duplicate measurements.

proximately 890 000 measurements between 40° S and 60° N (Fig. 1a). The distribution of observations in time (Fig. 2) shows them to be relatively uniform during the 1970s and 1980s, with a dip in the 1990s and then another rise after 2002 with the onset of Argo sampling. Before the 1990s the data consist mainly of a combination of LEGOS and OSD. In more recent times, the data are dominated by Argo. The reduction in data availability in the late 1990s probably reflects delays by research institutions in submitting their data to their respective national data centers, which then submit them to the US NODC which produced the WOD05.

Each data source has a different method of measuring salinity and verifying its accuracy. In some cases (Argo, LEGOS and TAO-TRITON), the data were collected by single agencies or entities with relatively standardized techniques. The WOD05 however, is a compendium of data collected by a myriad of sources. Given the diversity of data sources, the large amount of data that were eventually used and the purpose, to calculate the seasonal harmonic, a unified approach to quality control was not possible. We adopted the data deemed acceptable by the providers' quality flags (when available), and rejected data that in subsequent analysis were obviously erroneous.

A question arises whether the recent addition of Argo data skews the results presented. The basic analyses of amplitude and phase were repeated using only the Argo dataset and using only non-Argo data with only a small difference in the results. The Argo data help fill in gaps in mid-ocean, especially in the northeastern North Pacific and eastern South Pacific. As Argo continues over the years, it will become clearer if the patterns depicted in this study are robust.

2.1.7 TAO/TRITON moorings

A separate independent analysis was carried out using near-surface TAO (Tropical Atmosphere-Ocean) mooring data. The near-surface instruments typically were deployed at a depth of 1 or 2 m. Salinities were extracted from the files where the quality flag provided by the TAO program was either 1 (“highest quality”) or 2 (“default quality”).

2.1.8 Evaporation

Evaporation data were taken from the OAFflux dataset of Yu et al. (2008). This dataset combines satellite retrievals with three reanalyses as input to the COARE 3.0 bulk algorithm (Fairall et al., 2003). The data include monthly values of evaporation from 1958–2006 in 1° squares. Yu et al. published maps of standard deviation for latent heat flux (their Fig. 17), showing values between about 2 and 26 W m^{-2} . Translated into evaporation this range is $9\text{--}90 \times 10^{-7} \text{ kg m}^{-2} \text{ s}^{-1}$, much smaller than the seasonal amplitudes that will be calculated later in this paper.

2.1.9 Precipitation

Precipitation data were taken from the Global Precipitation Climatology Project (GPCP) monthly merged precipitation analysis (Huffman et al., 1997; Adler et al., 2003) on a $2.5^\circ \times 2.5^\circ$ grid. Adler et al. published error fields for the precipitation, and included one example month. The error fields were not used in this study. Significance estimates of seasonal amplitude and phase were based on scatter from harmonic fits (Sect. 2.2).

2.1.10 Mixed-layer depth

Mixed-layer depths were obtained from the Ocean Mixed Layer Depth Climatology which is a monthly climatology of mixed-layer depth derived from World Ocean Database and World Ocean Circulation Experiment data. The climatology uses a temperature criterion of 0.2°C difference from 10 m depth to estimate the depth (de Boyer Montegut et al., 2004). Note that this is not a time series, but a seasonal climatology, with a single value for each month for each 2° square.

2.1.11 Surface currents

Surface currents are taken from the OSCAR current database. Currents are estimated in 1° bins from satellite altimetry and vector winds, validated from in situ sources where available (Bonjean and Lagerloef, 2002). Currents include both geostrophic and Ekman components.

2.1.12 Upwelling

Values of Ekman upwelling were obtained from QuickSCAT data from the NOAA Coastwatch program. Upwelling values were obtained every 3 days for the period 31 July 1997–16

July 2006 on a 0.25° grid. They were calculated as $w_e = \nabla \times \tau / (\rho f)$, where τ is the windstress, ρ the surface density and f the Coriolis parameter. CoastWatch processes wind velocities to wind stress following Smith (1988) and to wind stress curl after the method of Gill (1982). Upwelling is not calculated within $\pm 1^\circ$ of the equator. However, since we used 2.5° boxes in this study, we used the equator most values in our calculations for areas close to the equator.

2.2 Harmonic analysis

The simple harmonic analysis used in this paper closely follows the method of Emery and Thomson (2001; pp. 392–395). For SLS for example, the combined data (Sect. 2.1.6) were grouped into $2.5^\circ \times 2.5^\circ$ boxes. For each box with more than 10 observations, SLS was least squares fit to the function

$$S = S_0 + a_0 \cos(\omega t) + a_1 \sin(\omega t) + \varepsilon \quad (1)$$

where $\omega = 2\pi/365.25$ days. ε is a residual whose size is minimized in a least squares sense by choice of a_0 and a_1 . t is the time measured in days from 1 January of each year. The significance of the fit was determined using a standard *f*-test and considered significant when it exceeded 95%. The percent of variance explained by the fit (R^2) was determined as well. The amplitude of the seasonal cycle is $A = \sqrt{a_0^2 + a_1^2}$ and the phase in radians is $\varphi = \tan^{-1}(a_1/a_0)$. Only the first harmonic – one cycle per year – is included in the analysis presented in this paper. We tried the same set of calculations including the semi-annual harmonic in the least squares fit as well. The results were not much different. Some areas with significant seasonal cycles got a bit larger, but the extra harmonic did not make much difference to the basic results that will be presented. We also tried removing a linear trend before doing the harmonic fit, and again the results were only slightly different.

3 Results

3.1 Seasonal cycles of SLS and E-P

The amplitude of the seasonal cycle of SLS is generally between 0.1 and 0.5 (Fig. 3) in areas where it is significant. There are roughly five areas where a significant fit was obtained: An area stretching around the northern and western rim of the North Pacific (areas WP and NNP), a band going across the tropical Pacific from close to the equator in the west to about 10°N in the east (area TP), an area in the tropical South Pacific stretching across about 15°S west of 150°W and about 10°S east of 150°W (area SP) and a small area north of the Hawaiian Islands centered at about 30°N (area HI). The amplitudes reach 0.5 and over in the eastern Pacific, the East China Sea, the Japan Sea and the Arafura

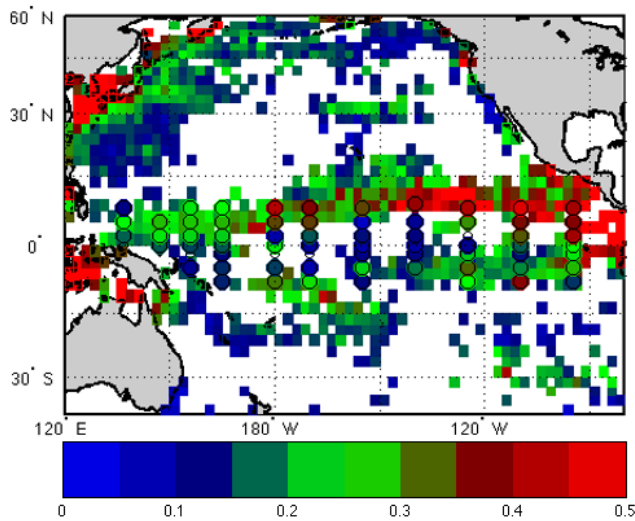


Fig. 3. Amplitude of the seasonal cycle of SLS from the combined dataset. Color scale is shown at bottom. Areas with no fill had observations, but from those observations no significant seasonal component was found. Seasonal cycles from TAO/TRITON moorings are shown in circles near the equator. Small empty circles indicate that mooring data were examined, but no significant seasonal cycle was found for that mooring.

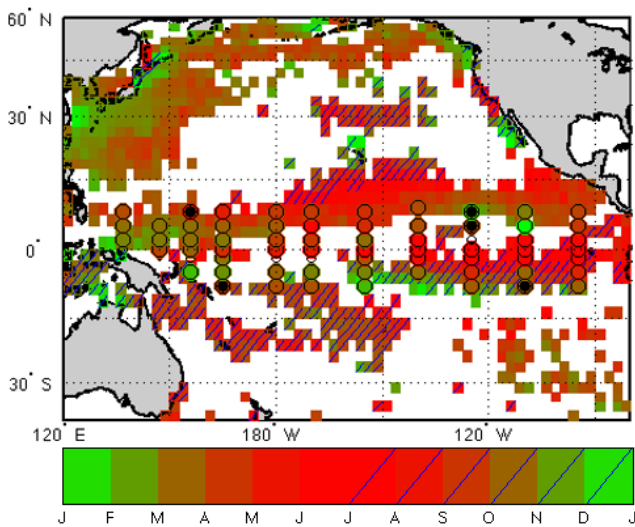


Fig. 4. As in Fig. 3, but for the phase. Color scale is shown at bottom with units of months, indicating the month of maximum SLS. Light blue slashes mean maximum SLS occurred during the second half of the year. For TAO/TRITON moorings a dark black dot in the middle indicates maximum SLS in the second half of the year.

Sea between New Guinea and Australia. Most squares with significant fits had amplitudes between 0.1 and 0.3.

There are large areas of the Pacific where there were data, but no significant seasonal cycle of SLS, blank areas in Fig. 3. There tended to be fewer data in the blank areas,

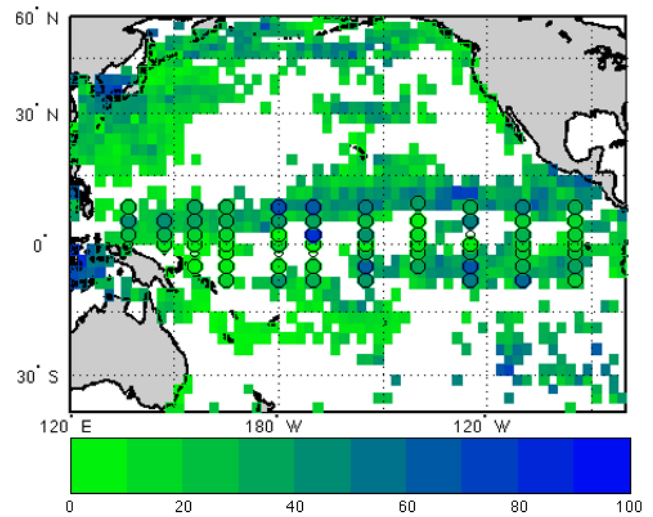


Fig. 5. As in Fig. 3, but for percent of variance explained, R^2 . Color scale is shown at bottom with units of %, indicating the fraction of variance explained by the seasonal cycle in each location.

a median of 189 observations in blank squares vs. 322 in non-blank squares. Perhaps as the Argo program fills in with more data, the seasonal cycles will be better defined in those areas. More likely, the blank areas in Fig. 3 do not have a statistically significant seasonal cycle.

The phase (Fig. 4) shows the distinction between each of the areas mentioned above. In areas WP and NNP, the maximum salinity occurs in late winter or early spring. In area TP, the maximum occurs in early- to mid- (Northern Hemisphere) summer. In area SP, the maximum occurs mostly in late (Southern Hemisphere) winter/early spring (August/September), but the timing is quite variable. In area HI, the maximum occurs in the late summer and fall.

The percent of variance (Fig. 5) of squares with a significant fit ranges from 10–20% up to nearly 100%. Area TP shows the highest percent of variance explained indicating that the seasonal is the main component of SLS variation in this area. Other areas with high values of percent of variance are south of the Aleutian Islands, and the marginal areas of the Sea of Japan and the Arafura Sea.

For area TP, the results closely match those of Delcroix et al. (2005) and Delcroix et al. (1996). In particular Delcroix et al. (2005) show an area of high R^2 in the eastern tropical Pacific, centered near 10° N and an area of good fit in the western tropical North Pacific, nearer to the equator. In both cases, the month of maximum salinity found here agrees with that shown by Delcroix et al. (1996). Amplitudes found here appear to be somewhat less than those found by Delcroix et al. For our results in the western tropical Pacific, the salinity varies in almost opposite phase to the central Pacific. The month of maximum salinity is near July around 180°, and moves toward earlier in the year both to the east and west of there. In agreement with this, Delcroix et al. (1996) show

an area in the western Pacific of nearly opposite phase. Gouriou and Delcroix (2002) also found similar results when they examined SLS variability in this region ($10\text{--}25^\circ\text{S}$ – 160°E – 140°W). They found a seasonal mode with an amplitude of about 0.5 pss and maximum salinity in September.

Area SP in the South Pacific in part corresponds to the South Pacific Convergence Zone (SPCZ), which stretches from the warm pool at 0° , 150°E to 30°S , 130°W (Vincent, 1994). The seasonal cycle of SLS under the SPCZ has an amplitude of $\sim 0.1\text{--}0.3$ and a maximum in austral winter/spring (Figs. 3, 4). The amplitude and phase agree well with the values found by Delcroix et al. (2005) along ship tracks in the central and western Pacific. In contrast to the maximum in SLS variability related to the ITCZ, there are gaps in the SLS amplitude underneath the SPCZ in the western South Pacific (Fig. 3). This could be related to the fact that the SPCZ is wider and more diffuse than the ITCZ, and that the seasonal amplitudes of precipitation are generally smaller in the SPCZ. The SP region continues eastward along about 10°S to the eastern boundary. The seasonal amplitudes in the eastern SP region are similar to those under the SPCZ, though the phasing in the eastern SP region is more variable (Figs. 3, 4).

The results presented here also match with those of Hires and Montgomery (1972) who measured seasonal variability along a track from Honolulu to Pago Pago. This track crosses the equator at approximately 165°W and slopes northeastward toward Honolulu at 158°W . They found a maximum amplitude of SLS seasonal variability at about 10°N . The minimum salinity comes in November and the amplitude is about 0.6.

For the northern North Pacific (area NNP), Ren and Riser (2009) looked at the area $45\text{--}50^\circ\text{N}$, $155\text{--}140^\circ\text{W}$. The amplitude of SLS they found, about 0.1 pss, is close to what we found. The SLS balance in the area was found to be mostly between SLS tendency and precipitation. The Coast Guard (1982) showed semi-annual variability in SSS at Ocean Station November (30°N , 140°W) from July 1966–June 1974. However, no attempt was made in that study to assess the significance of the signal. Xie and Arkin (1997) show global maps of seasonal precipitation based on the algorithm of Xie and Arkin (1996) over the years 1979–1995. Their maps show that the Alaskan gyre and northeast Pacific do get a large seasonal cycle in precipitation, with maximum rainfall in the January–March time period. We find a maximum in salinity in this area during March–May, suggesting that other processes besides precipitation must be important.

Seasonal cycles calculated from TAO moorings are similar to those from the station/float data (Figs. 3, 4 and 5). Significant seasonal variability is found throughout the tropical Pacific, with larger amplitudes in the northeastern area under the ITCZ. We compared the amplitudes and phases derived from TAO data and those from the main SLS dataset (Sect. 2.1.6) in the same areas. The two datasets had a correlation of 0.68 (amplitude) and 0.73 (phase). As an example of a comparison of the two datasets, we looked at

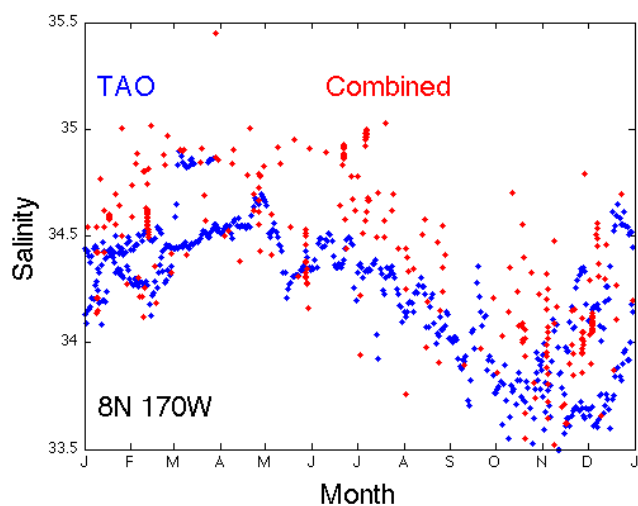


Fig. 6. Example of the seasonal cycle in the $2.5^\circ \times 2.5^\circ$ box centered at 8°N , 170°W . In blue are TAO mooring data from that location and in red are the combined SLS data from that box. Data are displayed by month to emphasize the seasonal cycle.

the TAO mooring at 8°N , 170°W (Fig. 6). This shows the two datasets vary in phase and exhibit a very similar seasonal cycle, with maximum SLS in April–May, minimum in October–November and amplitude of about 0.5.

It is possible that the ENSO cycle has a significant affect on seasonality of the SLS. To try to understand this, we ran the harmonic analysis of Figs. 3–5 for only ENSO years (1972–1973, 1976–1977, 1982–1983, 1986–1987, 1991–1992, 1997–1998, 2002–2003 and 2006–2007. 1 June–31 May for each pair of years (McPhaden and Zhang, 2009)), and for all data but excluding ENSO years. For the non-ENSO years, we found little difference in the results. For the ENSO years, there were some small differences. The seasonal cycles in the South Pacific mostly disappear, as do the ones in the northern and northeastern North Pacific. It is not clear how much of the difference is due to the use of ENSO-year data and how much to the greatly reduced size of the dataset.

Maps of E-P, E and P shows that most of the Pacific has significant seasonal variability in at least one of these quantities (Fig. 7). The seasonal cycle of E-P consists of the combined seasonal cycles of E and P. The seasonal cycle of E is the dominant component in the western North Pacific, while P is generally dominant elsewhere. The areas with the maximum amplitude of E-P are in the western North Pacific near Japan and to the east, an area east of the Philippines, an area between New Guinea and Australia and an area along the ITCZ at $\sim 10^\circ\text{N}$.

The maximum of E-P occurs in mid-winter near Japan, in spring along the ITCZ and in late Southern Hemisphere winter in the western South Pacific. In a regime where seasonal SLS variability is dominated by E-P, we would expect

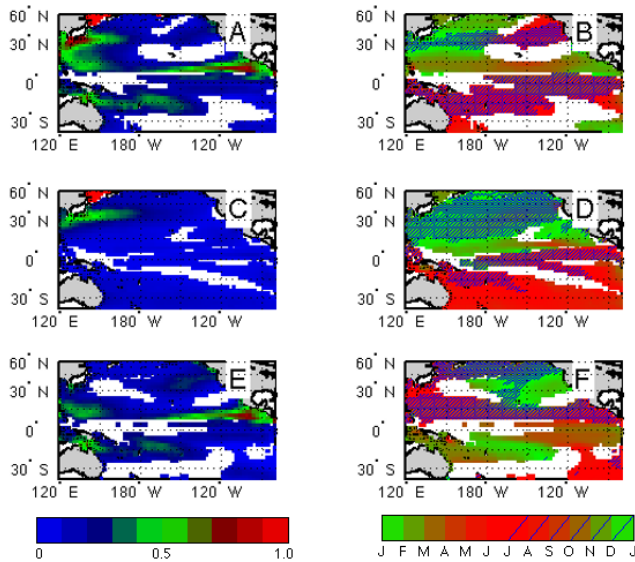


Fig. 7. Amplitude (left column) and phase (right column) of the seasonal cycle of (a) and (b) E-P, (c) and (d) evaporation and (e) and (f) precipitation. Panels (e) and (f) present the same information as Adler et al. (2003) Fig. 10. Color scale for panels (a), (c) and (e), is shown below panel (e) with units of $10^{-4} \text{ kg m}^{-2} \text{ s}^{-1}$. Color scale for panels (b), (d) and (f) is shown below panel (f). Phase scale indicates month of maximum E-P, evaporation or precipitation. Light blue slashes mean maximum SLS occurred during the second half of the year. White or blank areas indicate that enough data existed, but no significant seasonal cycle was found.

approximately a three month time lag between the maximum of E-P and the maximum of SLS (DH91; Hires and Montgomery, 1972; Fig. 4). This is more or less the case in most areas where seasonal cycles of both quantities exist. The phase of E shows maximum values throughout the North Pacific in late fall/early winter. The phase of P is more complicated, with a band across the tropical Pacific around 10°N with maximum precipitation in late summer/early fall.

3.2 Seasonal balance of SLS terms

Ignoring turbulent vertical diffusion which is difficult to reliably estimate, a simple equation describing SLS is given by Delcroix et al. (1996)

$$\frac{\partial S}{\partial t} = \frac{S_0(\text{E-P})}{h} - \mathbf{u} \cdot \nabla S - w \frac{\partial S}{\partial z} \quad (2)$$

where S_0 is the yearly average SLS, h is the mixed layer thickness, $\mathbf{u} = (u, v)$ is the horizontal velocity, w the vertical velocity and z the vertical coordinate. Each of the terms in Eq. (2) can be expressed in terms of the seasonal harmonic as in Eq. (1).

In the third term, $\mathbf{u} \cdot \nabla S$, we can express each of \mathbf{u} and S as a mean ($\bar{\mathbf{u}}$) and seasonally varying (u') part. The term can then be broken up into 1) seasonal advection of the mean salinity ($\bar{\mathbf{u}} \cdot \nabla \bar{S}$), 2) mean advection of the seasonally varying

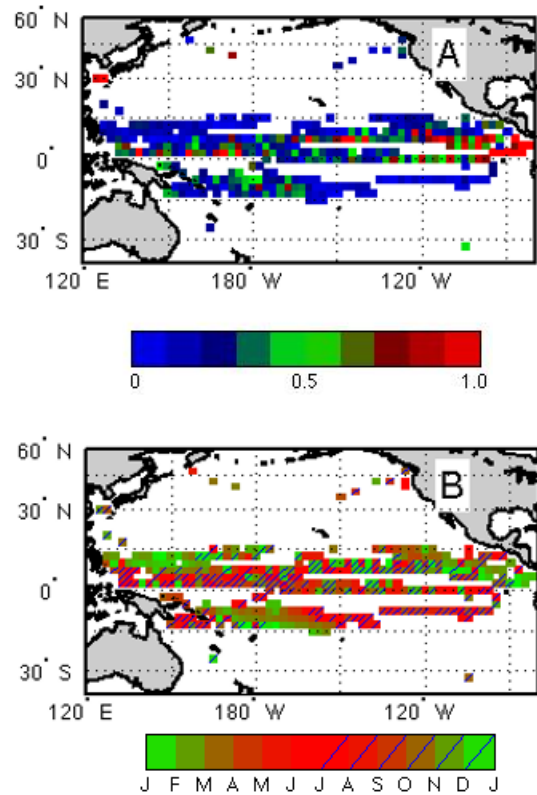


Fig. 8. (a) Amplitude of the $u' \cdot \nabla \bar{S}$ term in Eq. (2). Color scale is shown with units $10^{-7} \text{ pss s}^{-1}$. (b) Phase of the $u' \cdot \nabla \bar{S}$ term in Eq. (2). Color scale is shown indicating month of maximum value of the $u' \cdot \nabla \bar{S}$ term. White or blank areas over the ocean indicate that enough data existed, but no significant seasonal cycle was found.

salinity ($\bar{\mathbf{u}} \cdot \nabla \bar{S}$), and 3) seasonal advection of the seasonally varying salinity ($u' \cdot \nabla \bar{S}$). We will make no attempt here to depict 2) and 3). Calculation of these requires computation of the spatial gradient of salinity as a function of time, and then fitting those gradients to a sinusoidal function (as in Eq. 1). We deemed that doing this with the available data was not possible with any degree of confidence, especially with Argo data which are collected in quasi-random times and places. We do show the amplitude and phase of $u' \cdot \nabla \bar{S}$ (Fig. 8). The variability in this quantity is concentrated near the equator and underneath the ITCZ where there is a significant seasonal cycle of current. The amplitude and especially the phase are highly variable. This is due to the fact that the seasonal variability is in the zonal current but the SLS gradient vector points mostly in the meridional direction, making the dot product of the two close to zero. The advection shown in Fig. 8 is mainly zonal with some meridional component in the eastern Pacific.

The map of the amplitude of the seasonal cycle of SLS (Fig. 3) is the same as the map of the amplitude of the seasonal cycle of $\frac{\partial S}{\partial t}$ but using the scale of Fig. 8 (Delcroix et al., 1996). The phase of $\frac{\partial S}{\partial t}$ is the same as that of S (Fig. 4), but shifted backward in time by 3 months (Fig. 9).

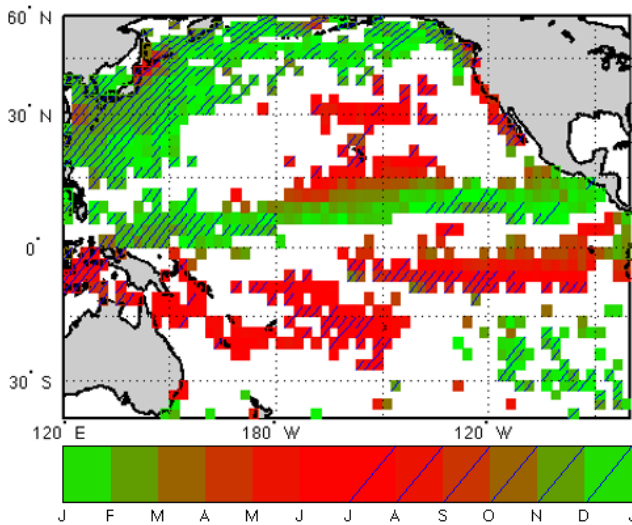


Fig. 9. Phase of the seasonal cycle of $\partial S/\partial t$ from the combined dataset. This figure presents the same information as Fig. 4 (without the TAO/TRITON data), shifted backward in time by 3 months. Color scale is shown at the bottom.

The seasonal cycle of the $\frac{S_0(E-P)}{h}$ term of Eq. (2) (Fig. 10) largely follows E-P (Figs. 7a, b). Seasonal variations of mixed-layer thickness were not large enough in most areas to alter the basic seasonal variation of this term. The term is strongest under the ITCZ in the eastern tropical North Pacific where it is driven by seasonal variations in rainfall, and in the western North Pacific where evaporation is the dominant process. Comparison of the figures showing the terms of Eq. (2) (Figs. 3, 8, 9 and 10) indicate some rough agreement between them in amplitude and phase. In areas where there is a significant seasonal cycle of $\frac{\partial S}{\partial t}$ it matches or nearly matches that of $\frac{S_0(E-P)}{h}$.

Similar to the advection term, we calculated the entrainment, the last term of Eq. (2), as 1) the seasonal variation of vertical velocity times the mean vertical gradient ($w' \frac{\partial S'}{\partial z}$) and 2) the mean vertical velocity times the seasonally varying vertical gradient ($\bar{w} \frac{\partial S'}{\partial z}$). The mean vertical salinity gradient was calculated from the World Ocean Atlas 2009 between the surface and the bottom of the mixed-layer. The seasonal vertical salinity gradient was calculated as the seasonal cycle of SLS minus $S(h_m)$ divided by h_m , $\frac{\partial S'}{\partial z} = \frac{(SLS - S(h+m))}{h_m}$, where h_m is the depth of the annual average mixed-layer (as calculated from the data presented in Sect. 2.1.10) plus 30 m. Seasonal vertical velocities were calculated from combining the upwelling (w_e ; Sect. 2.1.12) and the vertical motion of the mixed-layer depth ($\frac{\partial h}{\partial t}$; Sect. 2.1.10), $w = w_e + \frac{\partial h}{\partial t}$. Term 2) was found to be negligible over the entire Pacific. The median value of the amplitude was 20 times less than the median of the values of the seasonal cycle of $\frac{\partial S}{\partial t}$. Term 1) was mostly negligible, except for a small area in the eastern Tropical Pacific between 2.5 and 7.5° N (Fig. 11). Interestingly, this area

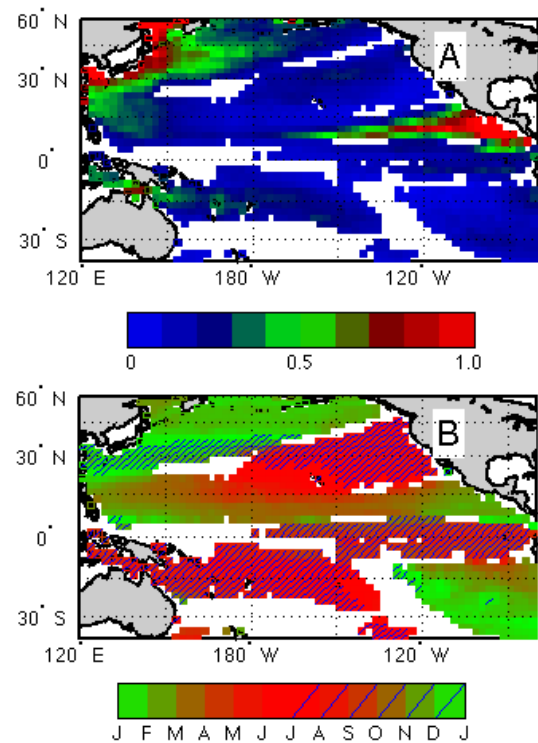


Fig. 10. (a) Amplitude and (b) phase of the seasonal cycle of $\frac{S_0(E-P)}{h}$ from Eq. (2). White or blank areas indicate that enough data existed, but no significant seasonal cycle was found. Color scale for panel (a) is shown with units of 10^{-7} pss. Color scale for panel (b) is shown. Units are months indicating maximum value of $\frac{S_0(E-P)}{h}$.

coincides with a meridional gap in the seasonal cycle of SLS (Fig. 3). This suggests that seasonal variation of E-P is balanced by entrainment in this small area. The amplitude of the entrainment is large in the area close to the coast of Central America, the Costa Rica Dome (Hoffman et al., 1981). The phase indicates the maximum of $w' \frac{\partial S'}{\partial z}$, or a minimum freshening of the surface layer in this area as the mean vertical gradient of salinity is negative (S increases with depth).

To get a better sense of the seasonal cycle on a regional scale, we calculated it over the areas as shown in Fig. 12, with results displayed in Table 1. The areas were chosen to be representative of the areas discussed in Sect. 3.1, WP, NNP, TP and SP. In all the areas shown except the South Pacific the amplitude and phase of the $\frac{S_0(E-P)}{h}$ and $\frac{\partial S}{\partial t}$ terms are similar. Phases are within two months and amplitudes within $1-2 \times 10^{-8}$ pss/s, indicating rough balance between the terms. The tropical South Pacific area is the one where the largest discrepancy occurs, with no significant seasonal signal at all in $\frac{S_0(E-P)}{h}$. The differing natures of the seasonal cycles are illustrated in Fig. 13, in which we show all the SLS data for each area, plotted as if they were collected in a single year, with monthly averages also displayed. The seasonal cycles in

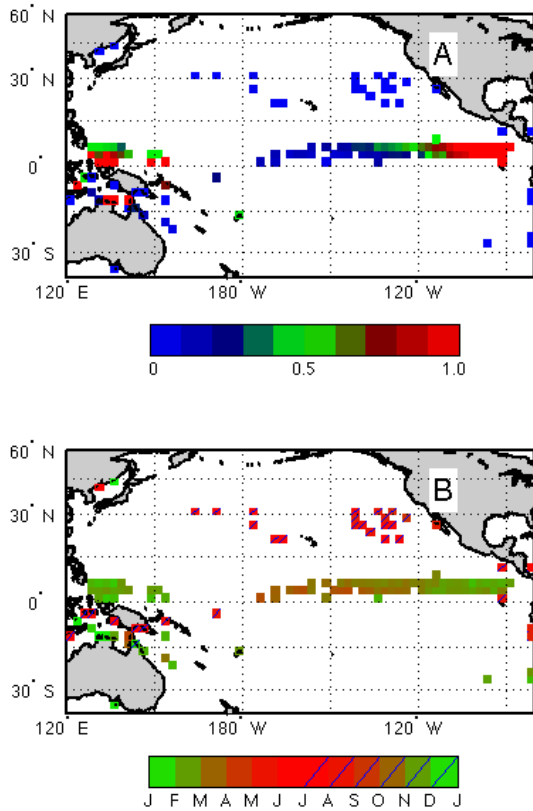


Fig. 11. Seasonal amplitude (a) and phase (b) of the entrainment term, $w' \frac{\partial S}{\partial z}$. White or blank areas indicate that enough data existed, but no significant seasonal cycle was found. Color scale for panel (a) is shown with units of 10^{-7} pss. Color scale for panel (b) is shown. Units are months indicating maximum value of $w' \frac{\partial S}{\partial z}$.

the tropical North Pacific and the northern North Pacific are sinusoidal, with SLS maxima in March/April and April/May respectively. The seasonal variations in the South Pacific and western North Pacific are more driven by a number of low outliers in the summer season in each case, giving maximum SLS values in the winter.

4 Discussion

The seasonal variability of SLS in the Pacific has been studied, using SLS and E-P data along with surface currents and mixed-layer depths. Maps of SLS seasonal cycles show limited areas where they are significant and large areas of the central oceans where they are not. The lack of seasonal variation of salinity in large areas of the Pacific may simply be due to a lack of sufficient data, and as Argo data become more abundant, many of the gaps in Fig. 3 will be filled in and the seasonal cycle better defined. Nevertheless, we were able to quantify and characterize the variability in the areas where it was most obvious, the western North Pacific boundary and mode water formation area, underneath the ITCZ in

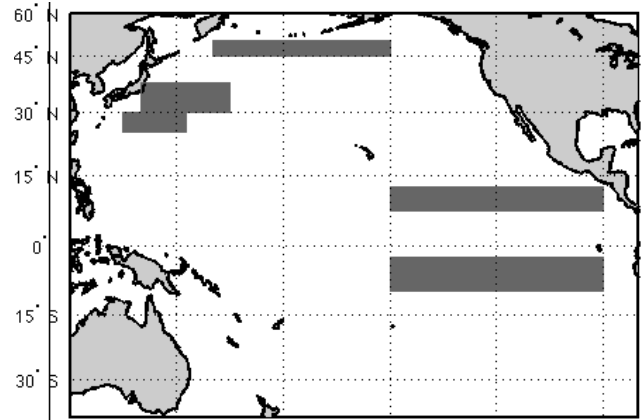


Fig. 12. Averaging areas as described in Table 1.

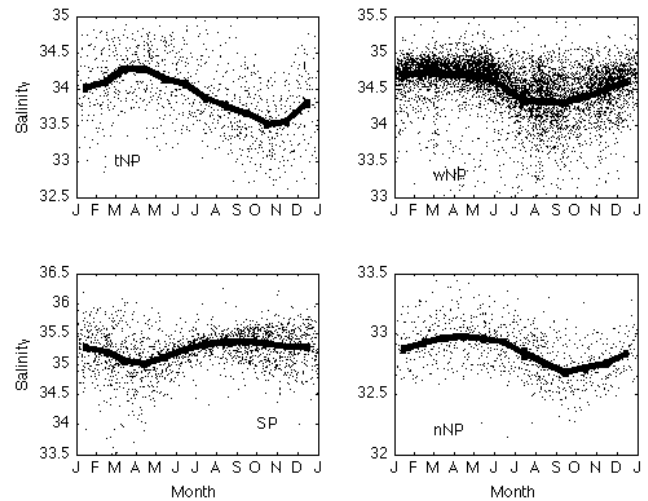


Fig. 13. SLS for the areas depicted in Fig. 12 and Table 1, plotted as a single year. Note that y-axis limits are different for each panel. Lettering in the bottom of each panel corresponds to areas described in Table 1. Dots are individual measurements, with only 10% of points plotted for clarity. Solid curves are monthly averages.

the eastern tropical Pacific, in the low-latitude eastern South Pacific, in the northern North Pacific and in some of the western marginal seas. In many areas, there is a seasonal balance between E-P and changing SLS.

Large amplitude changes in SLS in the western North Pacific likely play a significant role in the mode water formation process. Until now, much has been made of the way that density increases in this area in the wintertime leading to a thickening mixed-layer (e.g. Bingham, 1992). In most studies, decreased temperature has been considered as the main factor driving increased density. However, the present study suggests that seasonal variability in salinity, shown here to have just the right phase, could contribute significantly to mode water formation as well. At a base salinity of 35 and temperature of 15 °C, a seasonal cycle of 0.5 in salinity is

Table 1. Amplitudes and phases of seasonal constituents shown in the first line in areas shown in Fig. 11. Amplitudes are in units of 10^{-8} pss/s. Phases are in months, 1 = 1 January, 2 = 1 February, etc., and indicate the month of maximum value. Phase values in parentheses are dates of maximum salinity in each area and correspond approximately with the peaks of the curves in Fig. 11. Error bounds represent 95% confidence intervals found through a propagation of errors calculation.

Area	$\frac{dS}{dt}$		$S_0 \frac{(E-P)}{h}$	
	Amplitude	Phase	Amplitude	Phase
Northern Tropical Pacific	7.1 ± 0.2	$1.29 (4.29) \pm 0.07$	7.0 ± 0.1	2.88 ± 0.03
Western North Pacific	4.5 ± 0.1	$11.99 (2.99) \pm 0.04$	4.9 ± 0.1	12.74 ± 0.04
Southern Tropical Pacific	2.8 ± 0.1	$7.03 (10.03) \pm 0.10$	not significant	not significant
Northern North Pacific	2.9 ± 0.2	$1.17 (4.17) \pm 0.14$	3.2 ± 0.05	2.0 ± 0.03

the density equivalent of a seasonal cycle of temperature of about 2°C . The extra densification provided by salinity may be enough to create the extremely thick mixed layers seen in this area in late winter.

Seasonal advection was seen to play a minimal role in the salinity balance except perhaps in the tropics. However, the difficulty of doing the calculation of the mean advection of the seasonally varying salinity makes this conclusion very uncertain. The one place where advection clearly does play an important role is in the Costa Rica Dome area off Central America. Here, seasonally varying currents cross a sharp slanting SLS front which cuts northwest-southeast between 120 and 90°W . DH91 emphasized the role of meridional Ekman advection on the mean SLS, noting that the meridional maximum of precipitation is displaced slightly equatorward of the minimum of the mean SLS, attributing this displacement to advection. Delcroix et al. (1996) briefly discussed the potential role of seasonal advection of SLS by the north equatorial countercurrent, concluding it might possibly be significant. The value they give for the possible contribution, $2.5 \times 10^{-2} \text{ month}^{-1}$, is approximately equivalent to $0.1 \times 10^{-7} \text{ pss s}^{-1}$ as presented here and similar in magnitude to our results (Fig. 8).

Entrainment was found to be negligible over most of the Pacific, except for a small area in the eastern tropical Pacific. The far eastern part of this area of enhanced entrainment, the Costa Rica Dome, contains the thinnest mixed-layer of the entire Pacific, about 20 m thick on average (Kara et al., 2003). With such a thin mixed-layer one would expect that oceanic processes might be as important as surface forcing in regulating the SLS on the seasonal scale (Chang, 1993). Indeed, the amplitudes of the entrainment, SLS tendency, atmospheric forcing and horizontal advection terms are all large in this region. The seasonal SLS balance in this region is more complex than over the rest of the ocean, and would be a good area for future study.

The tropical Pacific Ocean is an important region climatically because it is the spawning ground for El Niño and the Southern Oscillation (ENSO). Understanding and predicting

ENSO and its global consequences requires a better understanding of the background conditions on which ENSO develops. In particular, the mean seasonal cycle has a strong influence on the character of ENSO variability through nonlinear interactions as demonstrated in intermediate and general coupled ocean-atmosphere circulation models (e.g., Chang et al., 1995; Guilyardi, 2006). The coupling of the ocean and atmosphere that gives rise to both the seasonal cycle and ENSO time scale variations in the Pacific depends on feedbacks between surface winds and sea surface temperatures (SST). The evolution of ENSO is also strongly influenced by changes in upper ocean heat content and potential energy (Jin, 1997; Brown and Fedorov, 2010). Salinity variations can affect these processes through their influence on upper ocean stratification, mixed layer heat storage, and SST (e.g., Ando and McPhaden, 1997; Reynolds et al., 1998; Maes et al., 2005). Thus, documenting the variations in and the causes for the mean seasonal cycle of surface salinity is an important step towards developing a comprehensive understanding of seasonal-to-interannual climate variability originating in the tropical Pacific.

This work has important implications for the SMOS and Aquarius satellite missions. Aquarius is supposed to deliver surface salinity measurements with accuracies of $0.1\text{--}0.2$ pss with a spatial resolution of $100\text{--}300\text{ km}$ and a temporal resolution of $7\text{--}30$ days (Lagerloef et al., 2008). There are areas in the Pacific with seasonal amplitudes this large and predictable phase, the ITCZ and the western North Pacific, along with some of the western marginal seas. The signals the satellite sees in these areas should be among the first to emerge from the data stream. Thus, these areas will make good test beds for the satellite missions and would be good candidates for intensive calibration and validation activities.

Acknowledgements. Funding provided by NASA as part of the Ocean Salinity Science Team program under grant # NNX09AU70G. Argo data were collected and made freely available by the International Argo Project and the national initiatives that contribute to it (<http://www.argo.net>). Argo is a pilot programme of the Global Ocean Observing System. Argo data were extracted from the NODC

Argo data repository (<http://www.nodc.noaa.gov/argo/>). WOD05 data were obtained from the NODC website (http://www.nodc.noaa.gov/OC5/WOD/pr_wod.html). EPIC data were obtained from the EPIC program website (<http://www.epic.noaa.gov>). OSCAR Surface currents provided courtesy of the OSCAR Project Office (<http://www.oscar.noaa.gov>). LEGOS data were provided by the French Sea Surface Salinity Observation Service (<http://www.legos.obs-mip.fr/en/observations/sss/>). QuickSCAT data were provided by the NOAA CoastWatch Program and Remote Sensing Systems Inc. (<http://coastwatch.pfeg.noaa.gov/erddap/griddap/erdQSstress3day.html>) OAFflux data were obtained at the OAFflux website (<http://oafux.who.edu/>). GPCP data were obtained from the program website (<http://precip.gsfc.nasa.gov/>). Mixed-layer depth climatology data were obtained here (<http://www.locean-ipsl.upmc.fr/~cdblod/mld.html>). PMEL publication no. 3553. JISAO contribution number 1827.

Edited by: S. Josey

References

- Adler, R. F., Huffman, G. J., Chang, A., Ferraro, R., Xie, P., Janowiak, J., Rudolf, R., Schneider, U., Curtis, S., Bolvin, D., Gruber, A., Susskind, J., Arkin, A., and Nelkin, E.: The Version 2 Global Precipitation Climatology Project (GPCP) Monthly Precipitation Analysis (1979–Present), *J. Hydrometeorol.*, 4, 1147–1167, 2003.
- Ando, K. and McPhaden, M. J.: Variability of surface layer hydrography in the tropical Pacific Ocean, *J. Geophys. Res.*, 102, 23063–23078, 1997.
- Antonov, J., Seidov, D., Boyer, T. P., Locarnini, R. A., Mishonov, A. V., and Garcia, H. E.: World Ocean Atlas 2009, Volume 2: Salinity, NOAA NESDIS Report 69, 184 pp., 2010.
- Berger, M., Camps, A., Font, J., Kerr, Y., Miller, J., Johannssen, J., Boutin, J., Drinkwater, M. R., Skou, N., Floury, N., Rast, M., Rebhan, H., and Attema, E.: Measuring Ocean Salinity with ESA's SMOS Mission, *ESA Bull.*, 111, 113–121, 2002.
- Bingham, F.: The Formation and Spreading of Subtropical Mode Water in the North Pacific, *J. Geophys. Res.*, 97, 11177–11189, 1992.
- Bonjean, F. and Lagerloef, G. S.: Diagnostic Model and Analysis of the Surface Currents in the Tropical Pacific Ocean, *J. Phys. Oceanogr.*, 32(10), 2938–2954, 2002.
- Boyer, T., Levitus, S., Antonov, J., Conkright, M., O'Brien, T., and Stephens, C.: World Ocean Atlas 1998 Volume 5: Salinity of the Pacific Ocean, 166 pp., Silver Spring, MD, 1998.
- Boyer, T. P. and Levitus, S.: Harmonic Analysis of Climatological Sea Surface Salinity, *J. Geophys. Res.*, 107(C12), doi:10.1029/2001JC000829, 2002.
- Brown, J. N. and Fedorov, A. V.: How much energy is transferred from the winds to the thermocline on ENSO time scales?, *J. Climate*, 23, 1563–1580, 2010.
- Chang, P.: Seasonal Cycle of Sea Surface Temperature and Mixed Layer Heat Budget in the Tropical Pacific Ocean, *Geophys. Res. Lett.*, 20(19), 2079–2082, 1993.
- Chang, P., Ji, L., Wang, B., and Li, T.: Interactions between the Seasonal Cycle and El Niño–Southern Oscillation in an Intermediate Coupled Ocean–Atmosphere Model, *J. Atmos. Sci.*, 52, 2353–2372, 1995.
- Coast Guard: Oceanographic observations : North Pacific Ocean Station November, July 1966–June 1974 and Pacific standard monitoring sections, P3, P4, P5, and P6, Oceanographic Report No. CG 373-82, US Department of Transportation, Washington D.C., 63 pp., 1982.
- de Boyer Montegut, C., Madec, G., Fischer, A. S., Lazar, A., and Iudicone, D.: Mixed layer depth over the global ocean: An examination of profile data and a profile-based climatology, *J. Geophys. Res.*, 109, C12003, doi:10.1029/2004JC002378, 2004.
- Delcroix, T. and Henin, C.: Seasonal and interannual variations of sea surface salinity in the Tropical Pacific Ocean, *J. Geophys. Res.*, 96(C12), 22135–22150, 1991.
- Delcroix, T., Henin, C., Porte, V., and Arkin, P.: Precipitation and Sea-surface Salinity in the Tropical Pacific, *Deep-Sea Res. I*, 43(7), 1123–1141, 1996.
- Delcroix, T., McPhaden, M., Dessier, A., and Gouriou, Y.: Time and space scales for sea surface salinity in the tropical oceans, *Deep-Sea Res.*, 52(5), 787–813, 2005.
- Emery, W. and Thomson, R.: Data Analysis Methods in Physical Oceanography, Second and Revised Edition, 658 pp., Elsevier Science Ltd., 2001.
- Fairall, C. W., Bradley, E. F., Hare, J., Grachev, A. A., and Edson, J. B.: Bulk parameterization on air–sea fluxes: Updates and verification for the COARE algorithm, *J. Climate*, 16, 571–591, 2003.
- Foltz, G. R. and McPhaden, M. J.: Seasonal Mixed Layer Salinity Balance of the Tropical North Atlantic Ocean, *J. Geophys. Res.*, 113, C02013, doi:10.1029/2007JC004178, 2008.
- Gill, A. E.: Atmosphere–Ocean Dynamics, 662 pp., Academic Press, New York, 1982.
- Guilyardi, E.: El Niño–mean state–seasonal cycle interactions in a multi-model ensemble, *Clim. Dynam.*, 26, 329–348, 2006.
- Gouriou, Y. and Delcroix, T.: Seasonal and ENSO Variations of Sea Surface Salinity and Temperature in the South Pacific Convergence Zone during 1976–2000, *J. Geophys. Res. (C Oceans)*, 107(C12), 3185, doi:10.1029/2001JC000830, 2002.
- Hanawa, K. and Talley, L. D.: Chapter 5.4 Mode Waters, in: Ocean Circulation and Climate, edited by: Siedler, G., Church, J., and Gould, J., Academic Press, New York, 2001.
- Hires, R. I. and Montgomery, R. B.: Navifacial Temperature and Salinity along the Track from Samoa to Hawaii, 1957–1965, *J. Mar. Res.*, 30(2), 177–200, 1972.
- Hoffman, E. E., Busalacchi, A. J., and O'Brien, J. J.: Wind Generation of the Coast Rica Dome, *Science*, 215, 552–554, 1981.
- Huffman, G. J., Adler, R. F., Arkin, A., Chang, A., Ferraro, R., Gruber, A., Janowiak, J., Joyce, R. J., McNab, A., Rudolf, R., Schneider, U., and Xie, P.: The Global Precipitation Climatology Project (GPCP) Combined Precipitation Data Set, *B. Amer. Meteorol. Soc.*, 78, 5–20, 1997.
- Jin, F. F.: An Equatorial Ocean Recharge Paradigm for ENSO. Part I: Conceptual Model, *J. Atmos. Sci.*, 54, 811–829, 1997.
- Johnson, E., Lagerloef, G. S., Gunn, J., and Bonjean, F.: Surface salinity advection in the tropical oceans compared with atmospheric freshwater forcing: A trial balance, *J. Geophys. Res. (C Oceans)*, 107(C12), doi:10.1029/2001JC001122, 2002.
- Johnson, D., Boyer, T. P., Garcia, H. E., Locarnini, R. A., Mishonov, A. V., Pitcher, M. T., Baranova, M. T., Antonov, J. I., and Smolyar, I.: World Ocean Database 2005 Documentation, 163 pp., US

- Government Printing Office, Washington, D.C., 2006.
- Kara, A. B., Rochford, P. A., and Hurlburt, H. E.: Mixed Layer Depth Variability over the Global Ocean, *J. Geophys. Res.*, 108(C3), 3079, doi:10.1029/2000JC000736, 2003.
- Lagerloef, G. S., Colomb, F. R., LeVine, D. M., Wentz, F., Yueh, S., Ruf, C., Lilly, J., Gunn, J., Chao, Y., deCharon, A., Feldman, G., and Swift, C.: The Aquarius/SAC-D Mission: Designed to Meet the Salinity Remote-sensing Challenge, *Oceanogr.*, 20(1), 68–81, 2008.
- Levitus, S., Burgett, R., and Boyer, T. P.: World Ocean Atlas 1994 Volume 3: Salinity, NESDIS Report, 99 pp., Washington D.C., 1994.
- Maes, C., Picaut, J., and Belamari, S.: Importance of the Salinity Barrier Layer for the Buildup of El Niño, *J. Climate*, 18, 104–118, 2005.
- McPhaden, M. J. and Zhang, X.: Asymmetry in zonal phase propagation of ENSO sea surface temperature anomalies, *Geophys. Res. Lett.*, 36, L13703, doi:10.1029/2009GL038774, 2009.
- Ren, L. and Riser, S.: Seasonal salt budget in the north-east Pacific Ocean, *J. Geophys. Res.*, 114, C12004, doi:10.1029/2009JC005307, 2009.
- Reynolds, R. W., Ji, M., and Leetmaa, A.: Use of salinity to improve ocean modeling, *Phys. Chem. Earth*, 23, 543–553, 1998.
- Reverdin, G., Frankignoul, C., Kestenare, E., and McPhaden, M.: Seasonal variability in the surface currents of the equatorial Pacific, *J. Geophys. Res.*, 99(C10), 20323–20344, 1994.
- Roemmich, D., Johnson, G. C., Riser, S., Davis, R. E., Gilson, J., Owens, W. B., Garzoli, S., Schmid, C., and Ignaszewski, M.: Argo Program, The: Observing the Global Ocean with Profiling Floats, *Oceanogr.*, 22(2), 35–43, 2009.
- Smith, S. D.: Coefficients for sea surface wind stress, heat flux, and wind profiles as a function of wind speed and temperature, *J. Geophys. Res.*, 93(C12), 15467–15472, 1988.
- Vincent, D. G.: The South Pacific Convergence Zone (SPCZ): A Review, *Mon. Weather Rev.*, 122, 1949–1970, 1994.
- Woodgate, R. A., Aagaard, K., and Weingartner, T. J.: Monthly temperature, salinity and transport variability of the Bering Strait through flow, *Geophys. Res. Lett.*, 32, L04601, doi:10.1029/2004GL021880, 2005.
- Xie, P. and Arkin, P. A.: Analysis of global monthly precipitation using gauge observations, satellite estimates, and numerical model predictions, *J. Climate*, 9, 840–858, 1996.
- Xie, P. and Arkin, P. A.: Global Precipitation: a 17 Year Analysis Based on Gauge Observations, Satellite Estimates and Numerical Model Outputs, *B. Am. Meteorol. Soc.*, 78, 2539–2558, 1997.
- Yu, L., Jin, X., and Weller, R.: Multidecade Global Flux Datasets from the Objectively Analyzed Air-sea Fluxes (OAFlux) Project: Latent and Sensible Heat Fluxes, Ocean Evaporation, and Related Surface Meteorological Variables, 64 pp., 2008.